Acta Mech 227, 1869–1884 (2016)
DOI 10.1007/s00707-016-1593-6

ORIGINAL PAPER

M. Mirzaei · Y. Kiani

Nonlinear free vibration of temperature-dependent sandwich beams with carbon nanotube-reinforced face sheets

Received: 22 August 2015 / Revised: 12 February 2016 / Published online: 25 March 2016

Abstract In this research, large amplitude free vibrations of a sandwich beam with stiff core and carbon nanotube (CNT)-reinforced face sheets are analysed. The distribution of CNTs across the thickness of the face sheets may be uniform or functionally graded. The equivalent single- layer theory of Timoshenko is used to construct the Hamiltonian of the beam under the von Kármán type of geometrical nonlinearity assumptions. A uniform temperature field through the beam is also included in the formulation. The Ritz method with polynomial basis functions is used to discrete the equations of motion and establish the matrix representation of the governing equations. A nonlinear eigenvalue problem is obtained and solved using a standard continuation procedure. After validating the developed solution method and formulation, parametric studies are conducted to examine the influences of thermal environment, core thickness-to-face sheet thickness ratio, boundary conditions, amplitude of vibrations, CNTs volume fraction and their distribution pattern. It is concluded that an increase in the volume fraction of CNTs results in higher fundamental frequency and decreases the nonlinear-to-linear frequency ratio.

1 Introduction

Due to their exceptional thermal, mechanical and electrical properties, carbon nanotubes (CNTs) stand as a potential candidate for the reinforcements of the composites [1], see e.g. [2–5]. The distribution of volume fraction of CNTs in a matrix may be combined with the concept of functionally graded (FG) materials. Consequently, as reinforcements, the distribution of CNTs in a matrix may be uniform or functionally graded [6]. Among the various mathematically possible distribution pattern of CNTs across the thickness, linearly graded patterns are more observed in the open literature due to their consistency with the fabrication procedures. Various researches are now available on the analysis of beams, plates and shells of various geometry made of functionally graded carbon nanotube-reinforced composites (FG-CNTRC). A survey on the available works on FG-CNTRC beams is provided below.

Lin and Xiang [7] performed an investigation on free vibrations of an FG-CNTRC beam based on both first-order and third- order shear deformable beam theories. In this research, the Ritz method is applied to discrete the motion equations and establish a standard eigenvalue problem. In the approximation of the displacement field, polynomial shape functions are used suitable for arbitrary in-plane and out-of-plane boundary conditions. Numerical results of this study depict the remarkable discrepancy of free vibration characteristics based on first- and third-order theories especially for beams with both edges clamped. Lin and Xiang [8] also

M. Mirzaei
Department of Mechanical Engineering, Faculty of Engineering, University of Qom, Qom, Iran

Y. Kiani (✉)
Faculty of Engineering, Shahrekord University, Shahrekord, Iran
E-mail: y.kiani@aut.ac.ir

performed an investigation on large amplitude free vibration of FG-CNTRC beams within the framework of first- and third-order beam theories consistent with the von Kármán type of geometrical nonlinearity. Instability regions of an FG-CNTRC beam subjected to harmonically varying axial force with non-uniform thickness are obtained by Pourasghar and Kamaian [9] using the classical beam theory formulations. In this research, in-plane vibrations and extensional-bending couplings are ignored, and the well-known fourth-order Euler beam equation is used to distinguish the parametric instability of the beam using the Bolotin approximation technique. The single governing equation is discretized by means of the generalized differential quadrature. The critical buckling temperature and thermal post-buckling equilibrium path of FG-CNTRC slender beams reinforced with two identical piezoelectric actuator layers are investigated by Rafiee et al. [10]. In this work, a straightforward method is developed to obtain the lateral deflection as a function of elevated temperature for a beam with both edges clamped. It is shown that, by adoption of a proper distribution pattern of CNTs, the critical buckling temperature of an FG-CNTRC may be enhanced. Furthermore, the influence of the applied actuator voltage to control the thermal buckling temperature of the FG-CNTRC is found to be small. Numerical results of this study reveal that FG-CNTRC beams with intermediate CNT volume fraction do not have, necessarily, intermediate buckling temperatures and post-buckling equilibrium paths. Implementing the generalized differential quadrature, compressive mechanical buckling and free vibration of FG-CNTRC beams is analysed by Yas and Samadi [11]. The first-order beam theory of Timoshenko is used to construct the governing equations. It is concluded that, by proper usage of distribution pattern of CNTs, the buckling resistance of the beam may be increased. Ansari et al. [12] applied the differential quadrature and Galerkin methods to analyse the nonlinear forced vibrations of a CNTRC beam subjected to lateral periodically varying load. Both uniform and graded patterns of CNTs across the beam thickness are included into the formulation. Von Kármán assumptions are established to construct the governing nonlinear dynamic equations.

Large amplitude free vibrations of FG-CNTRC beams using the polynomial Ritz formulation are investigated by Ke et al. [13]. Only a specific case of graded CNTs distribution and uniform distribution are considered in this work. The geometrical nonlinearity of this research is restricted to von Kármán type suitable for small strains and large deflections. It is shown that nonlinear frequency ratios of both simply supported-simply supported and clamped-simply supported FG-CNTRC beams are dependent on the sign of the vibration amplitudes, i.e., their nonlinear frequency ratio versus amplitude curves are unsymmetrical. Shen and Xiang [14] used a two-step perturbation technique to obtain the linear and nonlinear free vibration, nonlinear bending, thermal buckling and thermal post-buckling responses of FG-CNTRC beams where the temperature dependency of the constituents is also included. In this research, the interaction of a two-parameter elastic foundation is also considered. Numerical results of this study are limited to the case of FG-CNTRC beams with both edges simply supported in flexure with movable or immovable feature in in-plane direction. It is shown in this research that, for nonsymmetric distribution of CNTs, the equilibrium path of simply supported beams under even uniform heating is no longer of the bifurcation type. Based on the concept of physical neutral surface formulation, in which the stretching–bending coupling vanishes in the formulation, the governing nonlinear motion equations of on FG-CNTRC Timoshenko beam integrated with two identical piezoelectric layers are obtained by Rafiee et al. [15] and solved for nonlinear free vibration. The Galerkin method is used to construct the time-dependent ordinary differential equations. Time dependency of the motion equations is obtained using the multiple scales method. Using the first-order Bolotin technique, Ke et al. [16] obtained the instability regions of Timoshenko beams subjected to harmonically varying in-plane compressive loads. It is shown that, using FG-X type of CNTs distribution, the buckling load of an FG-CNTRC beam increases. A two-dimensional elasticity solution is developed by Alibeigloo and Liew [17] to obtain the stress analysis and free vibration characteristics of FG-CNTRC beams integrated with sensor and actuator piezoelectric layers. In this research, both ends of the beam are assumed to be simply supported. Navier solution through the beam length accompanied by the differential quadrature method through the beam depth is used to discretize the governing equations. Yang et al. [18] obtained the instability regions of a slender Euler–Bernoulli beam subjected to the simultaneous effects of uniform heating, constant voltage and periodically varying compressive force. The response of FG-CNTRC beams subjected to low- velocity impact of a single mass is analysed by Jam and Kiani [19]. Thermal environment effects are also included in this research. It is shown that the impact characteristics of FG-CNTRC beams are highly dependent to the distributed pattern and volume fraction of CNTs.

Unlike the case of single-layer FG-CNTRC beams, researches on sandwich beams with FG-CNTRC face sheets or host are rare in the open literature. Mirzaei and Kiani [20] investigated the thermal post-buckling and snap-through phenomenon of a thermally post-buckled sandwich beam with FG-CNTRC face sheets. In this research, the governing equations are obtained using the Ritz method and displacement control strategy along with the arc-length technique which is used to trace the equilibrium paths. Wu et al. [21] analysed the

free vibration and buckling loads of beams with stiff host layer and FG-CNTRC face sheets. Generalized differential quadrature is used to discretize the governing equation. Buckling loads and natural frequencies are obtained via the standard eigenvalue algorithm.

Literature on the analysis of FG-CNTRC plates is comprehensive. Liew and his co-authors examined the free vibration characteristics of FG-CNTRC plates [22–24]. They also investigated the dynamic response of an FG-CNTRC plate subjected to sudden lateral pressure [25], geometrically nonlinear large amplitude behaviour of FG-CNTRC plates within the framework of von Kármán plate theory [26–28], buckling [29], post-buckling [30], and parametric stability [31] of FG-CNTRC plates under in-plane compressive loads and stress analysis of laminated plates comprising FG-CNTRC layers [32].

Nonlinear free vibrations of a sandwich beam with CNTRC face sheets are examined in the present work. A sandwich beam is symmetric with respect to its mid-surface comprising an isotropic polymeric matrix and CNTs as reinforcements in the face sheets. Thermal environment effects are also included into the formulation. To account for large deformations, the von Kármán type of geometrical nonlinearity is also taken into account. Various types of volume fraction profile and various magnitudes of CNTs volume fraction are used for the face sheets. Only the uniform case of temperature distribution is considered. After establishing a nonlinear eigenvalue problem by applying the polynomial-based Ritz method into the Hamilton principle, an iterative displacement control procedure is used to obtain the nonlinear frequencies of the sandwich beam. After comparing the numerical results of this study with the available data in the open literature, numerical results are given for the sandwich beams with FG-CNTRC face sheets to examine the influence of boundary conditions, volume fraction of CNTs, graded profile of volume fraction of CNTs and host thickness-to-face thickness ratio.

2 Basic formulation

As an especial case of multilayered structures, sandwich structures consist of two stiff skins which are generally thin and a lightweight core which is thick. Face sheets in this study are made from functionally graded carbon nanotube-reinforced composites (FG-CNTRC). Generally, sandwich structures are mid-plane symmetric. Therefore, the thickness of each face sheet is considered as h_{f}. The core, on the other hand, is made from an isotropic homogeneous and relatively stiff material with thickness h_{H}. The total thickness of the sandwich beam, in such case, becomes $h = h_{\mathrm{H}} + 2h_{\mathrm{f}}$. A Cartesian coordinate system is applied to the beam where as usual x is located at one end of the beam mid-surface and z is perpendicular to the beam.

There are five different types of carbon nanotube-reinforced beams in the open literature. There are a uniformly distributed (UD) case and four different functionally graded (FG) cases, namely FG-V, FG-O, FG-X and FG-Λ. In this study, all of these types are considered for each of the face sheets. As a convention, for instance an FG-V sandwich beam is referred to a beam where the top face sheet is of the FG-V type. Due to the symmetry conditions, the other face sheet is of FG-Λ type.

It is assumed that CNTRC face sheets are made from a mixture of (10, 10) armchair single-walled carbon nanotubes (SWCNTs) as reinforcement, graded distribution in the thickness direction and a matrix which is assumed to be isotropic and homogeneous. The effective material properties of the two-phase composites, mixture of CNTs and an isotropic polymer, can be estimated according to the modified rule of mixtures as previously discussed by Shen [33,34] or the Mori–Tanaka scheme. Due to its simplicity, the modified rule of mixtures is used to obtain the equivalent properties of the CNTRC. To this end, the conventional rule of mixtures approach is modified by the introduction of efficiency parameters. These parameters are used to match the data obtained by the molecular dynamics approach and the rule of mixtures approach. Thus, the axial and shear modulus may be written as [20,35–37]

$$\begin{aligned} E_{11} &= \eta_1 V_{\mathrm{CN}} E_{11}^{\mathrm{CN}} + V_m E^m, \\ \frac{\eta_3}{G_{12}} &= \frac{V_{\mathrm{CN}}}{G_{12}^{\mathrm{CN}}} + \frac{V_m}{G^m} \end{aligned} \tag{1}$$

where in the above equations E_{11}^{CN} and G_{12}^{CN} are the elasticity modulus and shear modulus of SWCNTs, respectively. Besides, E^m and G^m indicate the corresponding properties of the isotropic matrix. The coefficients η_1 and η_3 are the so-called efficiency parameters to account for the scale-dependent material properties. These constants as mentioned earlier are evaluated by matching the effective properties of CNTRC obtained from the molecular dynamics simulations with those from the rule of mixtures [33]. Furthermore, in Eq. (1), V_{CN}

Table 1 Volume fraction of CNTs as a function of thickness coordinate for various cases of sandwich beams with CNTRC face sheets

CNTs distribution	V_{CN}, top face sheet	V_{CN}, bottom face sheet
UD CNTRC	V^*_{CN}	V^*_{CN}
FG-O CNTRC	$2V^*_{\mathrm{CN}}\left(1-\frac{\lvert 2z-h_{\mathrm{H}}-h_{\mathrm{f}}\rvert}{h_{\mathrm{f}}}\right)$	$2V^*_{\mathrm{CN}}\left(1-\frac{\lvert 2z+h_{\mathrm{H}}+h_{\mathrm{f}}\rvert}{h_{\mathrm{f}}}\right)$
FG-X CNTRC	$2V^*_{\mathrm{CN}}\frac{\lvert 2z-h_{\mathrm{H}}-h_{\mathrm{f}}\rvert}{h_{\mathrm{f}}}$	$2V^*_{\mathrm{CN}}\frac{\lvert 2z+h_{\mathrm{H}}+h_{\mathrm{f}}\rvert}{h_{\mathrm{f}}}$
FG-V CNTRC	$V^*_{\mathrm{CN}}\frac{2z-h_{\mathrm{H}}}{h_{\mathrm{f}}}$	$-V^*_{\mathrm{CN}}\frac{h_{\mathrm{H}}+2z}{h_{\mathrm{f}}}$
FG-Λ CNTRC	$V^*_{\mathrm{CN}}\frac{h_{\mathrm{H}}+2h_{\mathrm{f}}-2z}{h_{\mathrm{f}}}$	$V^*_{\mathrm{CN}}\frac{h_{\mathrm{H}}+2h_{\mathrm{f}}+2z}{h_{\mathrm{f}}}$

and V_m are the volume fractions of CNTs and matrix phase, respectively, which satisfy the condition [38–40]

$$V_{\mathrm{CN}}+V_m=1. \tag{2}$$

Uniform and four types of functionally graded distributions of the CNTs along the thickness direction of the nanocomposite face sheets are considered. The mathematical expression of CNTs volume fraction in each case of distribution is given in Table 1.

It is easy to check from Table 1 that UD and all of FG types will have the same value of volume fraction of CNTs. The effective Poisson ratio depends weakly on position [33] and is expressed as

$$\nu_{12}=V^*_{\mathrm{CN}}\nu^{\mathrm{CN}}_{12}+V_m\nu^m. \tag{3}$$

The longitudinal thermal expansion coefficient of the composite face sheets can be expressed by the Shapery model as [14,34]

$$\alpha_{11}=\frac{V_{\mathrm{CN}}E^{\mathrm{CN}}_{11}\alpha^{\mathrm{CN}}_{11}+V_mE^m\alpha^m}{V_{\mathrm{CN}}E^{\mathrm{CN}}_{11}+V_mE^m}. \tag{4}$$

In this study, a sandwich beam with FG-CNTRC face sheets is formulated within the framework of first-order shear deformable beam theory (FSDT). Based on the general concept of FSDT, axial and transverse displacement components of the beam, i.e. u and w, may be presented in terms of the axial displacement of the mid-plane u_0, transverse displacement of the mid-plane w_0 and rotation of cross section φ, as

$$\begin{aligned} u(x,z,t)&=u_0(x,t)+z\varphi(x,t),\\ w(x,z,t)&=w_0(x,t). \end{aligned} \tag{5}$$

Referring to the basic relations of strains and displacements according to the von Kármán assumptions suitable for small strains and large deflections, on a generic point of the beam, one may write the below equations for the strain components,

$$\begin{aligned} \varepsilon_{xx}&=\frac{\partial u}{\partial x}+\frac{1}{2}\left(\frac{\partial w}{\partial x}\right)^2=\frac{\partial u_0}{\partial x}+\frac{1}{2}\left(\frac{\partial w_0}{\partial x}\right)^2+z\frac{\partial\varphi}{\partial x},\\ \gamma_{xz}&=\frac{\partial u}{\partial z}+\frac{\partial w}{\partial x}=\varphi+\frac{\partial w_0}{\partial x}. \end{aligned} \tag{6}$$

And the constitutive equations of the beam when only axial and transverse components of the stress field are present may be written as

$$\begin{aligned} \sigma_{xx}&=Q_{11}(\varepsilon_{xx}-\alpha_{11}(T-T_0)),\\ \sigma_{xz}&=Q_{55}\gamma_{xz}. \end{aligned} \tag{7}$$

Here, T_0 is a reference temperature and T is the uniform temperature across the beam. Besides, Q_{11} and Q_{55} are evaluated in terms of the material constants as

$$\begin{aligned} Q_{11}&=E_{11},\\ Q_{55}&=G_{13}. \end{aligned} \tag{8}$$

The stress resultants of first-order shear deformable beam theory may be obtained easily upon integration of the stress components over the thickness. The stress resultants are easily obtained as

$$\begin{aligned} N_{xx} &= \int_{-h/2}^{+h/2} \sigma_{xx} \mathrm{d}z = A_{11}\left(\frac{\mathrm{d}u_0}{\mathrm{d}x} + \frac{1}{2}\left(\frac{\mathrm{d}w_0}{\mathrm{d}x}\right)^2\right) - N^{\mathrm{T}}, \\ M_{xx} &= \int_{-h/2}^{+h/2} z\sigma_{xx} \mathrm{d}z = D_{11}\frac{\mathrm{d}\varphi}{\mathrm{d}x}, \\ Q_{xz} &= K_{\mathrm{s}} \int_{-h/2}^{+h/2} \sigma_{xz} \mathrm{d}z = A_{55}\left(\varphi + \frac{\mathrm{d}w_0}{\mathrm{d}x}\right). \end{aligned} \tag{9}$$

In the above equation, K_{s} is the shear correction factor and is taken as $K_{\mathrm{s}} = \pi^2/12$ [12]. N^{T} is the induced stress resultant due to the uniform temperature rise loading which is equal to

$$N^{\mathrm{T}} = \int_{-h/2}^{+h/2} Q_{11}\alpha_{11}(T - T_0)\mathrm{d}z. \tag{10}$$

Note that no thermal moment is induced through the beam, since temperature is distributed uniformly through the beam and the thermo-mechanical properties of the sandwich beam are symmetric with respect to the mid-surface. Furthermore, in Eq. (9), A_{11}, $D_{11}$and A_{55} are the stretching, bending and shear stiffness, respectively, which may be obtained as

$$(A_{11}, D_{11}, A_{55}) = \int_{-h/2}^{+h/2} (Q_{11}, z^2 Q_{11}, Q_{55})\mathrm{d}z. \tag{11}$$

Again note that the stretching–bending coupling, B_{11}, is absent since the elasticity modulus is a symmetric function with respect to the mid-surface.

3 Solution method

Hamilton's principle is used to obtain the governing nonlinear equations of motion. For the case of absence of external loads, the statement of the Hamilton principle reads

$$\begin{aligned} &\delta \int_{t_0}^{t_1} (U - T)\mathrm{d}t = 0, \\ &t = t_1, t_2 : \delta u_0 = \delta w_0 = \delta\varphi = 0 \end{aligned} \tag{12}$$

where in the above equations t_1 and t_2 are arbitrary times. Besides, δU is the virtual strain energy per width of the beam which according to FSDT may be written as

$$\delta U = \int_0^L \int_{-h/2}^{+h/2} (\sigma_{xx}\delta\varepsilon_{xx} + K_{\mathrm{s}}\sigma_{xz}\delta\gamma_{xz})\,\mathrm{d}z\mathrm{d}x \tag{13}$$

and δT is the virtual kinetic energy of the beam per width which takes the form

$$\delta T = \int_0^L \int_{-h/2}^{+h/2} \rho\,(\dot{u}\delta\dot{u} + \dot{w}\delta\dot{w})\,\mathrm{d}z\mathrm{d}x. \tag{14}$$

While the complete set of dynamic equations and the associated boundary conditions may be obtained by applying the integration by parts technique to Eq. (12), energy-based methods also may be used to solve the equations associated with Eq. (12). Ritz method as a powerful tool is used extensively in the solution of linear and nonlinear problems arising in various fields of structural mechanics, see e.g. [41–44]. In the present research also, the Ritz method is used to discretize the governing system of equations. Beforehand, using the

general concept of the separation of variables method, time and space dependency of the primary variables may be separated. Accordingly, each of the functions u_0, w_0 and φ may be written in the next form [45]:

$$u_0(x,t) = \sum_{n=1}^{N} U_n(t) N_n^u(x),$$
$$w_0(x,t) = \sum_{n=1}^{N} W_n(t) N_n^w(x),$$
$$\varphi(x,t) = \sum_{n=1}^{N} \Phi_n(t) N_n^\varphi(x). \tag{15}$$

Here, N_n^u, N_n^w, N_n^φ are the shape functions which have to be chosen according to the boundary conditions. Besides, N is the number of terms which should be chosen to assure the convergence of the total displacements. In this study, the polynomial type of shape functions is used.

Substituting Eq. (15) into Eqs. (13) and (14) and integrating over thickness and length eliminates the dependency of the unknown variables to the spatial coordinates. Afterwards, the complete set of motion equations may be written in matrix representation as

$$\begin{bmatrix} \mathbf{M^{uu}} & \mathbf{M^{uw}} & \mathbf{M^{u\varphi}} \\ \mathbf{M^{wu}} & \mathbf{M^{ww}} & \mathbf{M^{w\varphi}} \\ \mathbf{M^{\varphi u}} & \mathbf{M^{\varphi w}} & \mathbf{M^{\varphi\varphi}} \end{bmatrix} \begin{Bmatrix} \ddot{\mathbf{U}} \\ \ddot{\mathbf{W}} \\ \ddot{\mathbf{\Phi}} \end{Bmatrix} + \begin{bmatrix} \mathbf{K^{uu}} & \mathbf{K^{uw}} & \mathbf{K^{u\varphi}} \\ \mathbf{K^{wu}} & \mathbf{K^{ww}} & \mathbf{K^{w\varphi}} \\ \mathbf{K^{\varphi u}} & \mathbf{K^{\varphi w}} & \mathbf{K^{\varphi\varphi}} \end{bmatrix} \begin{Bmatrix} \mathbf{U} \\ \mathbf{W} \\ \mathbf{\Phi} \end{Bmatrix} = \begin{Bmatrix} \mathbf{0} \\ \mathbf{0} \\ \mathbf{0} \end{Bmatrix}. \tag{16}$$

The nonlinear vibration problem is now governed by Eq. (16). In the above equation, the stiffness matrix is nonlinear since some of their elements are dependent on the unknown displacement vector $\mathbf{W}$. In linear vibration analysis, the nonlinear terms are dropped out of the stiffness matrix, and the system of Eq. (16) reduces to a standard eigenvalue problem using the fact that the problem obeys the separation of variables solution method whose time-dependent solution is a harmonic function with frequency ω. However, the nonlinear free vibration problem, in general, does not admit the separation of variables method. Consequently, the mode shape varies with respect to time and cannot be obtained using the general separation of variables idea. In the conventional solution of nonlinear free vibration problem, the time-dependent or the space-dependent solution of the nonlinear free vibration problem is assumed a priori based on the observation from the linear analysis. However, such solutions for beams with at least one edge clamped are not valid.

In some energy-based finite element formulations, the assumption $\ddot{\mathbf{X}} = -\omega^2\mathbf{X}$ is established. Of course, the numerical solutions of this method differ mainly from those obtained by assuming the space-dependent or the time-dependent solutions. In an alternative approach, Prathap and Varadan [46] reduced the continuum equivalent of Eq. (16) to a nonlinear eigenvalue problem by noting that the point of maximum amplitude (which is also the point of reversal of motion) is of special interest, and by defining certain properties of the time function at this point, i.e., $\ddot{\mathbf{X}}_{\max} = -\omega^2\mathbf{X}_{\max}$, Eq. (16) can be reduced to an equation in space alone, and the nonlinear eigenvalue problem that results can be solved for a numerically exact mode shape at maximum amplitude, and a corresponding eigenvalue, which can be derived in terms of ω^2, thus defined at the point of reversal of motion. In this paper, it is assumed that a point of maximum amplitude exists during the vibration and that this is also the point of reversal of motion of every point of the beam [47],

$$\begin{Bmatrix} \ddot{\mathbf{U}}_{\max} \\ \ddot{\mathbf{W}}_{\max} \\ \ddot{\mathbf{\Phi}}_{\max} \end{Bmatrix} = -\omega^2 \begin{Bmatrix} \mathbf{U}_{\max} \\ \mathbf{W}_{\max} \\ \mathbf{\Phi}_{\max} \end{Bmatrix}. \tag{17}$$

Substitution of Eq. (17) into Eq. (16) results in

$$\omega^2 \begin{bmatrix} \mathbf{M^{uu}} & \mathbf{M^{uw}} & \mathbf{M^{u\varphi}} \\ \mathbf{M^{wu}} & \mathbf{M^{ww}} & \mathbf{M^{w\varphi}} \\ \mathbf{M^{\varphi u}} & \mathbf{M^{\varphi w}} & \mathbf{M^{\varphi\varphi}} \end{bmatrix} \begin{Bmatrix} \mathbf{U}_{\max} \\ \mathbf{W}_{\max} \\ \mathbf{\Phi}_{\max} \end{Bmatrix} = \begin{bmatrix} \mathbf{K^{uu}} & \mathbf{K^{uw}} & \mathbf{K^{u\varphi}} \\ \mathbf{K^{wu}} & \mathbf{K^{ww}} & \mathbf{K^{w\varphi}} \\ \mathbf{K^{\varphi u}} & \mathbf{K^{\varphi w}} & \mathbf{K^{\varphi\varphi}} \end{bmatrix} \begin{Bmatrix} \mathbf{U}_{\max} \\ \mathbf{W}_{\max} \\ \mathbf{\Phi}_{\max} \end{Bmatrix} \tag{18}$$

or in a compact form

$$(\mathbf{K} - \omega^2\mathbf{M})\mathbf{X}_{\max} = 0 \tag{19}$$

Table 2 Appropriate p-Ritz shape functions associated with the boundary conditions (20)

shape function	C–C	C–S	S–S
N_n^u	$\left(\frac{x}{L}\right)^n\left(1-\frac{x}{L}\right)$	$\left(\frac{x}{L}\right)^n\left(1-\frac{x}{L}\right)$	$\left(\frac{x}{L}\right)^n\left(1-\frac{x}{L}\right)$
N_n^w	$\left(\frac{x}{L}\right)^n\left(1-\frac{x}{L}\right)$	$\left(\frac{x}{L}\right)^n\left(1-\frac{x}{L}\right)$	$\left(\frac{x}{L}\right)^n\left(1-\frac{x}{L}\right)$
N_n^φ	$\left(\frac{x}{L}\right)^n\left(1-\frac{x}{L}\right)$	$\left(\frac{x}{L}\right)^n$	$\left(\frac{x}{L}\right)^{n-1}$

where in the above matrix $\mathbf{K}$ is the nonlinear elastic matrix and $\mathbf{M}$ is the mass matrix whose elements are provided in the "Appendix". The elements of nonlinear elastic matrix are dependent to the unknown displacement components. The above equation is a nonlinear eigenvalue problem and should be solved iteratively with respect to displacement vector $\mathbf{X}_{\max}$. The procedure to solve this problem is mentioned next.

At first, a linear analysis should be carried out to obtain the linear frequencies and the associated mode shapes. To obtain the governing equations associated with the linear vibration, the elements of the elastic matrix are linearized. Equivalently, the linear frequency analysis is dominant when the nonlinear components of the elastic matrix are ignored. Solving the resulting equation as an eigenvalue problem, the natural frequencies and the associated mode shapes of the system follow. To obtain the nonlinear free vibration characteristics of the system, the following procedure should be carried out.

(i) An element of the displacement vector $\mathbf{X}_{\max}$ is assumed to be known. In this study, $W_{1,\max}$ is considered to be known.
(ii) The eigenvector associated with the linear analysis is scaled up according to the assumed displacement of step (i).
(iii) The nonlinear components of the elastic matrix are computed with the displacement vector of step (ii).
(iv) A linear eigenvalue analysis at this step may be done.
(v) Note that the obtained results at the end of step (iv) are just approximate because of step (ii). The eigenvector obtained by step (iv) is scaled up by the assumed displacement W_1.
(vi) The procedure of steps (iii) to (v) is performed iteratively to reach a converged frequency parameter and the associated eigenvector (mode shape). When convergence is achieved, the nonlinear frequency is obtained.

It should be pointed out that the complete set of boundary conditions may be obtained in the process of applying the Hamilton principle. For the two well-known cases of boundary conditions, i.e. clamped (C) and simply supported (S) boundary conditions, the following conditions should be satisfied at each edge:

$$\begin{aligned} &\mathrm{C}: u_0 = w_0 = \varphi = 0, \\ &\mathrm{S}: u_0 = w_0 = M_x = 0. \end{aligned} \tag{20}$$

The polynomial shape functions associated with the C–C, C–S and S–S type of boundary conditions are given by Ghiasian et al. [45]. Here C–S indicates a beam which is clamped at $x = 0$ and simply supported at $x = L$. The same shape functions are used in the present study and are given in Table 2.

4 Numerical results and discussion

The procedure outlined in the previous sections is used herein to study the nonlinear free vibration characteristics of sandwich beams with FG-CNTRC face sheets. In this section, at first, two comparison studies are conducted. Afterwards, parametric studies are performed to examine the influences of involved parameters. Unless otherwise stated, Poly (methyl methacrylate), referred to as PMMA, is selected for the matrix of face sheets with material properties $E^m = (3.52 - 0.0034T)$ GPa, $\nu^m = 0.34$, $\rho_m = 1150$ kg/m^3 and $\alpha^m = 45 \times 10^{-6}(1 + 0.0005\Delta T)$ 1/K. In the calculation of the elasticity modulus of the matrix, $T = T_0 + \Delta T$ where $T_0 = 300$ K is the reference temperature. (10, 10) armchair SWCNT is chosen as the reinforcements in the face sheet. Elasticity modulus, shear modulus, Poisson's ratio and thermal expansion coefficient of SWCNT are highly dependent on temperature. Shen and Xiang [14] reported these properties at four certain temperature levels, i.e., $T = 300$, 400, 500 and 700 K. The magnitudes of E_{11}, G_{12}, α_{11}, ρ and ν_{12} for (10, 10) armchair SWCNT at these four specific temperatures are given in Table 3.

Table 3 Thermo-mechanical properties of (10, 10) armchair SWCNT at specific temperatures [14,34,48,49]

$T(K)$	E_{11}^{CN} (TPa)	G_{12}^{CN} (TPa)	ν_{12}^{CN}	α_{11}^{CN} (10^{-6}/K)	ρ^{CN} (kg/m^3)
300	5.6466	1.9445	0.175	3.4584	2100
400	5.5679	1.9703	0.175	4.1496	2100
500	5.5308	1.9643	0.175	4.5361	2100
700	5.4744	1.9644	0.175	4.6677	2100

Han and Elliott [50] performed a molecular dynamics simulation to obtain the elastic properties of CNTRC made of PMMA matrix and (10, 10) armchair SWCNT. However, in their analysis the effective CNT diameter was chosen large, and therefore, their simulations were redone by Shen [33]. As stated earlier, two efficiency parameters are introduced in the rule of mixtures to account for the size dependency of the mechanical properties of the composite media. For three specific constants of CNT volume fraction, these constants are chosen to equal the obtained magnitudes of E_{11} and G_{12} from the proposed modified rule of mixtures with those obtained by Han and Elliott [50]. For $V_{CN}^{*} = 0.12$, these constants are $\eta_1 = 0.137$ and $\eta_3 = 0.715$. For $V_{CN}^{*} = 0.17$, these constants are $\eta_1 = 0.142$ and $\eta_3 = 1.138$. For $V_{CN}^{*} = 0.28$, these constants are $\eta_1 = 0.141$ and $\eta_3 = 1.109$. It is of worth noting that, in the subsequent numerical studies, G_{13} is set equal to G_{12}.

It is assumed that the core is made of Ti-6Al-4V whose properties are dependent on temperature according to the following expressions: [51]:

$$\begin{aligned} E^{c} &= 122.56(1 - 4.586 \times 10^{-4} T)\,\text{GPa}, \\ \alpha^{c} &= 7.5788(1 + 6.638 \times 10^{-4} T - 3.147 \times 10^{-6} T^{2}) \times 10^{-6}\,1/\text{K}, \\ \rho^{c} &= 4429\,\text{kg/m}^3, \\ \nu^{c} &= 0.325. \end{aligned} \tag{21}$$

Unless otherwise stated, a sandwich beam is operating at reference temperature. In all of the numerical examples, the frequency parameter is defined by $\Omega = \omega L\sqrt{\rho^{c}/E_{ref}^{c}}$ where E_{ref}^{c} is the elasticity modulus of the core at reference temperature.

4.1 Comparison studies

Two comparison studies are presented in this section. For the first comparison study, the fundamental frequency parameter of a sandwich beam with FG-CNTRC face sheets is evaluated and compared with the results of Wu et al. [21]. In the analysis of Wu et al. [21], linear frequencies of a sandwich beam with Ti-6Al-4V core and FG-CNTRC face sheets are computed using the differential quadrature method. It should be pointed out that slight differences are observed in the mechanical properties of the core among the values of the present study and those of Wu et al. [21] which are ignored. In the analysis of Wu et al. [21], Poisson's ratio is chosen as $\nu_c = 0.342$ instead of $\nu_c = 0.325$ of this study. Also mass density is $\rho_c = 4430$ kg/m^3 instead of $\rho_c = 4429$ kg/m^3 which is chosen in this study. Furthermore, in the evaluation of the stiffness matrix in the analysis of Wu et al. [21] the effect of Poisson's ratio is included; however, this study does not take into account such effect in the stiffness matrix. Wu et al. [21] obtained the extensional stiffness using $Q_{11} = E_{11}(1 - \nu_{12}\nu_{21})^{-1}$. While in our research, as seen from Eq. (8), the effect of Poisson's ratio is ignored and $Q_{11} = E_{11}$ is taken into consideration. These slight differences, however, do not generate significant differences. For comparison study, a relatively thick beam with $L/h = 20$ and $h_H/h_f = 8$ is considered. Three different values of nanotube volume fraction are considered, and two types of boundary conditions are examined. Results are provided in Table 4. It is seen that reasonable agreement is observed at the onset of comparison.

For the second comparison study, the nonlinear-to-linear frequency ratio of a homogeneous isotropic beam with various boundary conditions is evaluated from the present approach, and results are compared with those obtained by Marur and Prathap [52]. Three different types of boundary conditions are considered. For the sake of comparison, a slender beam with length-to-thickness ratio $L/h = 100$ is considered and the thickness of face sheets is set equal to 0. In such case, the present formulation reduces to an isotropic homogeneous beam made of Ti-6Al-4V. Table 5 presents the ratio of nonlinear frequency to linear frequency ω_{nl}/ω_l for various values of maximum vibration amplitude. It is seen that excellent agreement is observed by the comparison of our results with those reported by Marur and Prathap [52] which guarantees the accuracy and correctness of the present formulation and solution procedure.

Table 4 A comparison of fundamental frequency parameter, Ω, of a sandwich beam with FG-CNTRC face sheets, $h_H/h_f = 8$ and $L/h = 20$

	$V^*_{CN} = 0.12$		$V^*_{CN} = 0.17$		$V^*_{CN} = 0.28$	
	UD	FG-V	UD	FG-V	UD	FG-V
C–C						
Present	0.3254	0.3305	0.3557	0.3623	0.4080	0.4171
Wu et al. [21]	0.3195	0.3240	0.3470	0.3530	0.3949	0.4032
Diff (%)	1.84	2.00	2.50	2.63	3.32	3.44
S–S						
Present	0.1416	0.1440	0.1557	0.1588	0.1803	0.1846
Wu et al. [21]	0.1432	0.1453	0.1560	0.1588	0.1785	0.1825
Diff (%)	1.11	0.89	0.19	0.00	1.01	1.15

Table 5 Nonlinear-to-linear frequency ratios of a slender beam ($L/h = 100$) made of an isotropic homogeneous material

W/h	C–C		C–S		S–S	
	Present	[52]	Present	[52]	Present	[52]
$1/\sqrt{12}$	1.0287	1.0283	1.0572	1.0582	1.1181	1.1180
$2/\sqrt{12}$	1.1112	1.1105	1.2130	1.2150	1.4143	1.4135
$3/\sqrt{12}$	1.2326	1.2336	1.4276	1.4368	1.8029	1.8027
$4/\sqrt{12}$	1.3832	1.3856	1.6912	1.6822	2.2362	2.2361
$5/\sqrt{12}$	1.5536	1.5574	1.9012	1.9180	2.6927	2.6925

Table 6 Fundamental frequency parameter, Ω, of sandwich beams with FG-CNTRC face sheets, $L/h = 20$ and S–S type of boundary conditions

	V^*_{CN}	UD	FG-Λ	FG-V	FG-X	FG-O
$h_H/h_f = 8$	0.12	0.1498	0.1473	0.1522	0.1498	0.1497
	0.17	0.1646	0.1613	0.1679	0.1647	0.1645
	0.28	0.1906	0.1859	0.1952	0.1908	0.1905
$h_H/h_f = 6$	0.12	0.1523	0.1484	0.1562	0.1525	0.1522
	0.17	0.1702	0.1651	0.1752	0.1704	0.1701
	0.28	0.2009	0.1939	0.2078	0.2012	0.2007
$h_H/h_f = 4$	0.12	0.1572	0.1503	0.1640	0.1576	0.1570
	0.17	0.1797	0.1708	0.1883	0.1802	0.1793
	0.28	0.2173	0.2053	0.2287	0.2179	0.2167

Table 7 Fundamental frequency parameter, Ω, of sandwich beams with FG-CNTRC face sheets, $L/h = 20$ and C–C type of boundary conditions

	V^*_{CN}	UD	FG-Λ	FG-V	FG-X	FG-O
$h_H/h_f = 8$	0.12	0.3359	0.3305	0.3412	0.3361	0.3357
	0.17	0.3682	0.3610	0.3752	0.3784	0.3680
	0.28	0.4240	0.4140	0.4337	0.4242	0.4237
$h_H/h_f = 6$	0.12	0.3414	0.3329	0.3497	0.3417	0.3411
	0.17	0.3802	0.3691	0.3909	0.3806	0.3798
	0.28	0.4457	0.4307	0.4601	0.4462	0.4452
$h_H/h_f = 4$	0.12	0.3519	0.3367	0.3664	0.3527	0.3512
	0.17	0.4003	0.3811	0.4185	0.4012	0.3994
	0.28	0.4796	0.4544	0.5032	0.4808	0.4784

4.2 Parametric studies

After performing comparison studies, parametric studies are done in this section to analyse the influences of involved parameters on the large amplitude free vibration of a sandwich beam with FG-CNTRC face sheets.

Tables 6, 7 and 8 present the fundamental frequency parameter of, respectively, S–S, C–C and C–S sandwich beams with FG-CNTRC face sheets. In each case, the length-to-total thickness ratio is set equal to $L/h = 20$.

Table 8 Fundamental frequency parameter, Ω, of sandwich beams with FG-CNTRC face sheets, $L/h = 20$ and C–S type of boundary conditions

	V^*_{CN}	UD	FG-Λ	FG-V	FG-X	FG-O
$h_{\mathrm{H}}/h_{\mathrm{f}} = 8$	0.12	0.2326	0.2288	0.2364	0.2328	0.2325
	0.17	0.2554	0.2503	0.2604	0.2560	0.2553
	0.28	0.2951	0.2880	0.3020	0.2952	0.2950
$h_{\mathrm{H}}/h_{\mathrm{f}} = 6$	0.12	0.2366	0.2306	0.2424	0.2368	0.2364
	0.17	0.2640	0.2561	0.2716	0.2643	0.2637
	0.28	0.3107	0.3000	0.3210	0.3111	0.3103
$h_{\mathrm{H}}/h_{\mathrm{f}} = 4$	0.12	0.2441	0.2334	0.2543	0.2446	0.2436
	0.17	0.2784	0.2647	0.2914	0.2791	0.2777
	0.28	0.3352	0.3174	0.3523	0.3362	0.3344

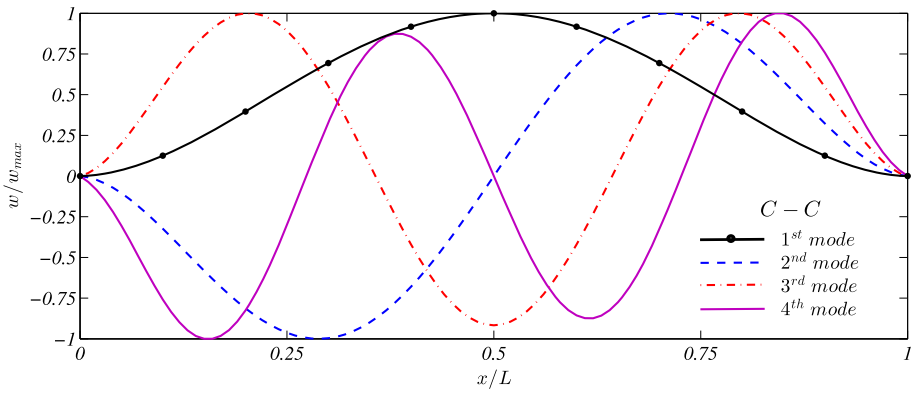

Fig. 1 First four mode shapes of C–C sandwich beam with FG-CNTRC face sheets. Volume fraction of CNT is $V^*_{\mathrm{CN}} = 0.17$, and distribution pattern is according to FG-V. Geometric characteristics of the beam are $L/h = 20$ and $h_{\mathrm{H}}/h_{\mathrm{f}} = 8$

Three different values are assumed for the thickness of the host layer to the thickness of the face sheet which are $h_{\mathrm{H}}/h_{\mathrm{f}} = 4$, 6 and 8. Besides, frequency parameters are provided for three different values of volume fraction of CNTs and five different cases of graded profile. As expected, in each case, the natural frequency of C–C beam is higher than the C–S beam, and the latter case is also higher than S–S beam. Such trend is expected due to the higher local flexural rigidity of a clamped edge in comparison with a simply supported one. In each case, the FG-V type of carbon nanotube distribution for the top face sheet results in a higher natural frequency parameter in comparison with the other types of distribution. Generally, it is concluded that the fundamental frequency of symmetric sandwich beams with FG-V type of CNTs distribution in the top face sheet is higher than, in order, FG-X, UD, FG-O and FG-Λ. However, differences of natural frequency for FG-X, UD, FG-O are hard to detect. From the results of these tables, it is concluded that, as the volume fraction of CNT in the face sheets increases, the fundamental natural frequency increases. The influence of thickness of host to thickness of face sheet is also observant since any increase in this ratio results in a decrease in the fundamental frequency. It may be concluded that, among the distribution profile, CNT volume fraction and host-to-face thickness ratio, the volume fraction is the most influential parameter on the natural frequency.

Figures 1, 2 and 3 depict the first four free vibration mode shapes of, respectively, C–C, C–S and S–S sandwich beams with FG-CNTRC face sheets. Length to total thickness is set equal to $L/h = 20$, and core to face thickness is assumed as $h_{\mathrm{H}}/h_{\mathrm{f}} = 8$. In these figures, the volume fraction is set equal to $V^*_{\mathrm{CN}} = 0.17$ and the distribution of CNTs in top face sheet obeys the FG-V pattern.

As the numerical results of Tables 6, 7 and 8 reveal, for FG-V pattern of CNTs distribution, the frequency parameter of a sandwich beam with CNTRC face sheets becomes maximum, and therefore, in the rest of this work only this kind of CNTs from the functionally graded type of distributions is taken into account.

Table 9 investigates the nonlinear-to-linear frequency ratio of an S–S sandwich beam with CNTRC face sheets. The distribution of CNTs along the thickness of the top face sheet is of the UD or FG-V type. Three different ratios are considered for core thickness to face sheet thickness, which are $h_{\mathrm{H}}/h_{\mathrm{f}} = 4$, 6 and 8. In each case, three different ratios are considered for the volume fraction of CNTs. As the numerical results of this table reveal, the linear fundamental frequency of the sandwich beam increases by either increasing CNT volume fraction or decreasing the host-to-face thickness ratio. It is seen that the fundamental frequency of a

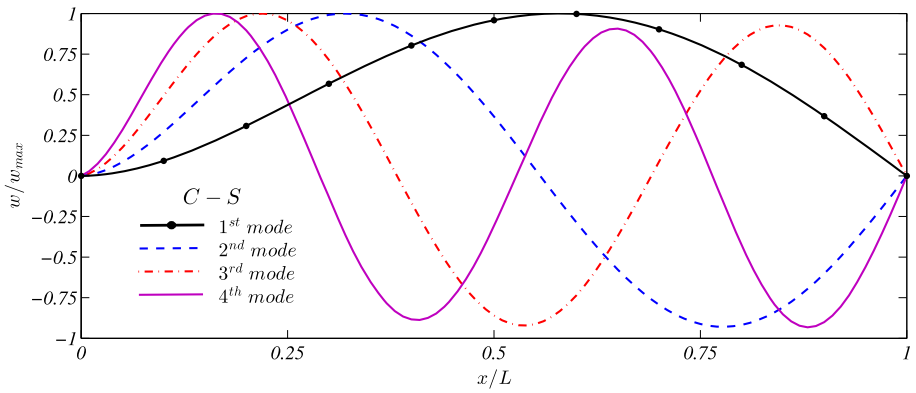

Fig. 2 First four mode shapes of C–S sandwich beam with FG-CNTRC face sheets. Volume fraction of CNT is $V^*_{\mathrm{CN}} = 0.17$ and distribution pattern is according to FG-V. Geometric characteristics of the beam are $L/h = 20$ and $h_{\mathrm{H}}/h_{\mathrm{f}} = 8$

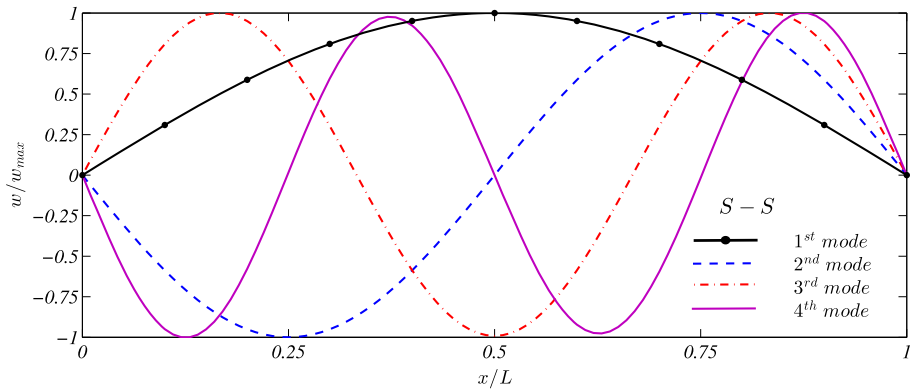

Fig. 3 First four mode shapes of S–S sandwich beam with FG-CNTRC face sheets. Volume fraction of CNT is $V^*_{\mathrm{CN}} = 0.17$ and distribution pattern is according to FG-V. Geometric characteristics of the beam are $L/h = 20$ and $h_{\mathrm{H}}/h_{\mathrm{f}} = 8$

Table 9 Nonlinear-to-linear frequency ratio $\omega_{\mathrm{nl}}/\omega_{\mathrm{l}}$ of sandwich beams with CNTRC face sheets, $L/h = 20$ and S–S type of boundary conditions

	$h_{\mathrm{H}}/h_{\mathrm{f}}$	V^*_{CN}	Ω	W/h				
				0.2	0.4	0.6	0.8	1
FG-V	8	0.12	0.1522	1.0585	1.2173	1.4435	1.7106	2.0022
		0.17	0.1679	1.0522	1.1954	1.4018	1.6477	1.9181
		0.28	0.1952	1.0447	1.1687	1.3500	1.5690	1.8120
	6	0.12	0.1562	1.0578	1.2149	1.4390	1.7038	1.9931
		0.17	0.1752	1.0509	1.1906	1.3925	1.6337	1.8992
		0.28	0.2078	1.0431	1.1629	1.3390	1.5522	1.7892
	4	0.12	0.1640	1.0563	1.2094	1.4285	1.6881	1.9722
		0.17	0.1883	1.0488	1.1832	1.3784	1.6123	1.8704
		0.28	0.2287	1.0413	1.1564	1.3261	1.5324	1.7624
UD	8	0.12	0.1498	1.0604	1.2238	1.4559	1.7292	2.0269
		0.17	0.1646	1.0543	1.2025	1.4155	1.6685	1.9459
		0.28	0.1906	1.0468	1.1762	1.3647	1.5915	1.8424
	6	0.12	0.1523	1.0607	1.2248	1.4577	1.7320	2.0306
		0.17	0.1702	1.0538	1.2009	1.4124	1.6638	1.9396
		0.28	0.2009	1.0460	1.1734	1.3593	1.5833	1.8312
	4	0.12	0.1573	1.0610	1.2259	1.4599	1.7351	2.0349
		0.17	0.1797	1.0534	1.1996	1.4098	1.6598	1.9343
		0.28	0.2173	1.0456	1.1719	1.3565	1.5789	1.8255

Table 10 Nonlinear-to-linear frequency ratio $\omega_{\mathrm{nl}}/\omega_{\mathrm{l}}$ of sandwich beams with CNTRC face sheets with $L/h = 20$, $V^*_{\mathrm{CN}} = 0.17$ and various boundary conditions

	$h_{\mathrm{H}}/h_{\mathrm{f}}$	Type	Ω	W/h				
				0.2	0.4	0.6	0.8	1
C–C	8	FG-V	0.3752	1.0130	1.0506	1.1101	1.1872	1.2808
		UD	0.3682	1.0135	1.0525	1.1138	1.1938	1.2904
	6	FG-V	0.3909	1.0126	1.0492	1.1073	1.1831	1.2690
		UD	0.3802	1.0134	1.0521	1.1132	1.1927	1.2863
	4	FG-V	0.4185	1.0121	1.0475	1.1031	1.1766	1.2618
		UD	0.4003	1.0131	1.0519	1.1124	1.1919	1.2860
C–S	8	FG-V	0.2604	1.0261	1.0996	1.2116	1.3507	1.5041
		UD	0.2554	1.0271	1.1034	1.2191	1.3625	1.5244
	6	FG-V	0.2716	1.0254	1.0976	1.2065	1.3427	1.4974
		UD	0.2640	1.0269	1.1030	1.2173	1.3605	1.5207
	4	FG-V	0.2914	1.0244	1.0937	1.1987	1.3305	1.4805
		UD	0.2784	1.0267	1.1020	1.2158	1.3581	1.5173
S–S	8	FG-V	0.1679	1.0522	1.1954	1.4018	1.6477	1.9181
		UD	0.1646	1.0543	1.2025	1.4155	1.6685	1.9459
	6	FG-V	0.1752	1.0509	1.1906	1.3925	1.6337	1.8992
		UD	0.1702	1.0538	1.2009	1.4124	1.6638	1.9396
	4	FG-V	0.1883	1.0488	1.1832	1.3784	1.6123	1.8704
		UD	0.1797	1.0534	1.1996	1.4098	1.6598	1.9343

sandwich beam with FG-V type of CNT is higher than of a sandwich beam with uniformly distributed CNTs. The investigation of nonlinear-to-linear frequency ratios takes into account the fact that this ratio decreases as the volume fraction of CNTs in the face sheets increases. Therefore, the nonlinear-to-linear frequency ratio of sandwich beams with $V^*_{\mathrm{CN}} = 0.12$ is higher than the case with $V^*_{\mathrm{CN}} = 0.17$, and the frequency ratio for the latter case is also higher than $V^*_{\mathrm{CN}} = 0.28$. The influence of core thickness to face thickness on the frequency ratio is not monotonic, and its increase may result in increasing or decreasing the frequency ratio. However, the effect of this ratio is ignorable. Besides, the ratio of nonlinear to linear frequency is dependent on the graded profile of CNTs across the thickness of face sheets and for sandwich beams with UD-CNTRC; this ratio is higher than for sandwich beams with FG-V CNTRC face sheets. This conclusion is similar to the findings of Wang and Shen [14] for the case of a sandwich plate with CNTRC face sheets.The effect of the graded profile, similar to core to face thickness influence, is ignorable.

The next parametric study aims to investigate the effect of boundary conditions on the nonlinear-to-linear frequency ratio of sandwich beams with CNTRC face sheets. Numerical results of this parametric study are provided in Table 10. In this table, for three different thickness ratios of the sandwich beam, i.e. $h_{\mathrm{H}}/h_{\mathrm{f}} = 8, 6$ and 4, two types of CNTs pattern, namely FG-V and UD, and three types of boundary conditions, the nonlinear-to-linear frequency ratio, are provided for some specific magnitudes of maximum amplitude. It is observed that for all types of boundary conditions and thickness ratio the fundamental frequency of a sandwich beam with FG-V CNTRC face sheets is higher than of those with UD-CNTRC face sheets. However, the discrepancy is small. On the other hand, the ratio of nonlinear to linear frequency is higher for uniform type of CNTs distribution. However, again, the difference of this ratio for FG-V and UD type of graded profiles is small. The nonlinear-to-linear frequency ratio is maximum for an S–S beam and is minimum for a C–C beam which is compatible with the results of Ke et al. [13] for the case of a single-layer FG-CNTRC beam.

The next parametric study is devoted to the examination of the thermal environment effect on the nonlinear-to-linear frequency ratio of a sandwich beam with CNTRC face sheets. In this example, both edges of the beam are considered to be clamped. The length-to-thickness ratio is set equal to 20, and the core to face thickness is considered as $h_{\mathrm{H}}/h_{\mathrm{f}} = 6$. Three different thermal environment cases are considered. Numerical results are tabulated in Table 11. It is seen from the results of this table that an increase in temperature level results in decreasing the fundamental frequency and also increases the nonlinear-to-linear frequency ratio. These conclusions are compatible with the findings of Shen and Xiang [14] for the case of a single CNTRC higher-order beam with both edges simply supported. For all of the studied cases of volume fraction and temperature level, it is worth noting that the fundamental frequency of a beam with FG-V CNTRC face sheet is higher than that of a beam with UD-CNTRC beam, whereas the nonlinear-to- linear frequency ratios of a sandwich beam with FG-V CNTRC beam are lower than those of the sandwich beam with UD-CNTRC beam in all the considered examples.

Table 11 Influence of thermal environment on nonlinear-on-linear frequency ratio $\omega_{\mathrm{nl}}/\omega_{\mathrm{l}}$ of sandwich beams with CNTRC face sheets, $L/h = 20$, $h_{\mathrm{H}}/h_{\mathrm{f}} = 6$, and C–C boundary conditions

	V^*_{CN}	Type	Ω	W/h				
				0.2	0.4	0.6	0.8	1
$T = 300$	0.12	FG-V	0.3497	1.0142	1.0556	1.1212	1.2053	1.3068
		UD	0.3414	1.0149	1.0586	1.1265	1.2150	1.3199
	0.17	FG-V	0.3909	1.0126	1.0492	1.1073	1.1831	1.2690
		UD	0.3802	1.0134	1.0521	1.1132	1.1927	1.2863
	0.28	FG-V	0.4601	1.0107	1.0421	1.0919	1.1571	1.2368
		UD	0.4457	1.0114	1.0448	1.0979	1.1673	1.2509
$T = 400$	0.12	FG-V	0.3328	1.0151	1.0590	1.1279	1.2163	1.3208
		UD	0.3242	1.0159	1.0621	1.1345	1.2269	1.3358
	0.17	FG-V	0.3744	1.0131	1.0514	1.1121	1.1910	1.2863
		UD	0.3634	1.0141	1.0546	1.1188	1.2014	1.3020
	0.28	FG-V	0.4438	1.0111	1.0435	1.0947	1.1628	1.2451
		UD	0.4290	1.0119	1.0465	1.1013	1.1732	1.2586
$T = 500$	0.12	FG-V	0.3216	1.0155	1.0605	1.1306	1.2214	1.3305
		UD	0.3128	1.0164	1.0639	1.1378	1.2330	1.3469
	0.17	FG-V	0.3631	1.0134	1.0525	1.1144	1.1944	1.2919
		UD	0.3519	1.0143	1.0560	1.1212	1.2062	1.3087
	0.28	FG-V	0.4320	1.0112	1.0441	1.0965	1.1654	1.2494
		UD	0.4171	1.0133	1.0474	1.1035	1.1769	1.2660

5 Concluding remarks

The large amplitude free vibration of a sandwich beam with FG-CNTRC face sheets in thermal environment is studied in the present work. The analysis is done employing a micromechanical model and a multi-scale approach which captures the length-scale property of the CNTs in face sheets. Both uniform and graded types of distributed CNTs are considered. Material properties of CNTs, matrix and host layer are all considered to be temperature dependent. Following the first-order equivalent single-layer theory for the sandwich beam, a Ritz-based formulation is developed upon the adoption of a polynomial type of shape functions suitable for immovable in-plane edges and clamped or simply supported out-of-plane edges. The resulting equations are rewritten in matrix representation and solved as a standard eigenvalue problem. Numerical results are provided for the influences of thermal environment, boundary conditions, core-to-face sheet thickness ratio, volume fraction of CNTs and distribution pattern of CNTs. The numerical results of this study reveal that:

- Due to the stiffer configuration of a clamped edge in comparison with a simply supported one, the natural frequency of a C–C sandwich beam with CNTRC face sheets is higher than of C–S beam, and the latter one is also higher than of an S–S sandwich beam.
- An increase in the volume fraction of CNTs results in higher natural frequency of a sandwich beam with CNTRC face sheets.
- Among the various graded profiles of the CNTs through the thickness of the face sheets, the frequency of a sandwich beam with FG-V CNTRC face sheet is maximum. Also a sandwich beam with FG-Λ CNTRC face sheet has the least natural frequency in comparison with the other graded patterns.
- Increasing the temperature through the beam with immovable edges results in a lower natural frequency.
- Increasing the thickness ratio decreases/increases the frequency of the sandwich beam. The nonlinear-to-linear frequency ratio increases as the thickness ratio increases.
- At a prescribed vibration amplitude, the nonlinear-to-linear frequency ratio is maximum for a beam with both edges simply supported and minimum for a beam with both edges clamped.
- The nonlinear-to-linear frequency ratio increases slightly with the increase in temperature.
- The nonlinear-to-linear frequency ratio of a sandwich beam with UD-CNTRC face sheets is slightly higher than the ratio for a sandwich beam with FG-V CNTRC face sheets.

Appendix

The elements of the elastic stiffness matrix which is presented previously in Eq. (16) are

$$\mathbf{K}^{\mathbf{uu}}_{\mathbf{mn}} = \int_0^L A_{11} \frac{\mathrm{d}N^u_m}{\mathrm{d}x} \frac{\mathrm{d}N^u_n}{\mathrm{d}x} \mathrm{d}x,$$
$$\mathbf{K}^{\mathbf{uw}}_{\mathbf{mn}} = \frac{1}{2} \int_0^L A_{11} \frac{\mathrm{d}N^u_m}{\mathrm{d}x} \frac{dw_0}{\mathrm{d}x} \frac{\mathrm{d}N^w_n}{\mathrm{d}x} \mathrm{d}x,$$
$$\mathbf{K}^{\mathbf{u}\boldsymbol{\varphi}}_{\mathbf{mn}} = 0,$$
$$\mathbf{K}^{\mathbf{wu}}_{\mathbf{mn}} = \int_0^L A_{11} \frac{\mathrm{d}N^w_m}{\mathrm{d}x} \frac{dw_0}{\mathrm{d}x} \frac{\mathrm{d}N^u_n}{\mathrm{d}x} \mathrm{d}x,$$
$$\mathbf{K}^{\mathbf{ww}}_{\mathbf{mn}} = \int_0^L \left(\frac{1}{2} A_{11} \frac{\mathrm{d}N^w_m}{\mathrm{d}x} \left(\frac{dw_0}{\mathrm{d}x} \right)^2 \frac{\mathrm{d}N^w_n}{\mathrm{d}x} + (A_{55} - N^{\mathrm{T}}) \frac{\mathrm{d}N^w_m}{\mathrm{d}x} \frac{\mathrm{d}N^w_n}{\mathrm{d}x} \right) \mathrm{d}x,$$
$$\mathbf{K}^{\mathbf{w}\boldsymbol{\varphi}}_{\mathbf{mn}} = \int_0^L A_{55} \frac{\mathrm{d}N^w_m}{\mathrm{d}x} N^{\varphi}_n \mathrm{d}x,$$
$$\mathbf{K}^{\boldsymbol{\varphi}\mathbf{u}}_{\mathbf{mn}} = 0,$$
$$\mathbf{K}^{\boldsymbol{\varphi}\mathbf{w}}_{\mathbf{mn}} = \int_0^L A_{55} N^{\varphi}_m \frac{\mathrm{d}N^w_n}{\mathrm{d}x} \mathrm{d}x,$$
$$\mathbf{K}^{\boldsymbol{\varphi}\boldsymbol{\varphi}}_{\mathbf{mn}} = \int_0^L \left(D_{11} \frac{\mathrm{d}N^{\varphi}_m}{\mathrm{d}x} \frac{\mathrm{d}N^{\varphi}_n}{\mathrm{d}x} + A_{55} N^{\varphi}_m N^{\varphi}_n \right) \mathrm{d}x.$$

Similarly, the elements of the mass matrix which is presented previously in Eq. (16) are

$$\mathbf{M}^{\mathbf{uu}}_{\mathbf{mn}} = I_1 \int_0^L N^u_m N^u_n \mathrm{d}x,$$
$$\mathbf{M}^{\mathbf{uw}}_{\mathbf{mn}} = 0,$$
$$\mathbf{M}^{\mathbf{u}\boldsymbol{\varphi}}_{\mathbf{mn}} = 0,$$
$$\mathbf{M}^{\mathbf{wu}}_{\mathbf{mn}} = 0,$$
$$\mathbf{M}^{\mathbf{ww}}_{\mathbf{mn}} = I_1 \int_0^L N^w_m N^w_n \mathrm{d}x,$$
$$\mathbf{M}^{\mathbf{w}\boldsymbol{\varphi}}_{\mathbf{mn}} = 0,$$
$$\mathbf{M}^{\boldsymbol{\varphi}\mathbf{u}}_{\mathbf{mn}} = 0,$$
$$\mathbf{M}^{\boldsymbol{\varphi}\mathbf{w}}_{\mathbf{mn}} = 0,$$
$$\mathbf{M}^{\boldsymbol{\varphi}\boldsymbol{\varphi}}_{\mathbf{mn}} = I_3 \int_0^L N^{\varphi}_m N^{\varphi}_n \mathrm{d}x.$$

References

1. Liew, K.M., Lei, Z.X., Zhang, L.W.: Mechanical analysis of functionally graded carbon nanotube reinforced composites: a review. Compos. Struct. **120**, 90–97 (2015)
2. Kundalwal, S.I., Meguid, S.A.: Effect of carbon nanotube waviness on active damping of laminated hybrid composite shells. Acta Mech. **226**, 2035–2052 (2015)
3. Ngabonziza, Y., Li, J., Barry, C.F.: Electrical conductivity and mechanical properties of multiwalled carbon nanotube-reinforced polypropylene nanocomposites. Acta Mech. **220**, 289–298 (2011)
4. Moradi-Dastjerdi, R., Pourasghar, A., Foroutan, M.: The effects of carbon nanotube orientation and aggregation on vibrational behavior of functionally graded nanocomposite cylinders by a mesh-free method. Acta Mech. **224**, 2817–2832 (2013)
5. Yanase, K., Moriyama, S., Ju, J.W.: Effects of CNT waviness on the effective elastic responses of CNT-reinforced polymer composites. Acta Mech. **224**, 1351–1364 (2013)
6. Shen, H.S.: Nonlinear bending of functionally graded carbon nanotube reinforced composite plates in thermal environments. Compos. Struct. **91**, 9–19 (2009)

7. Lin, F., Xiang, Y.: Vibration of carbon nanotube reinforced composite beams based on the first and third order beam theories. Appl. Math. Model. **38**, 3741–3754 (2014)
8. Lin, F., Xiang, Y.: Numerical analysis on nonlinear free vibration of carbon nanotube reinforcement composite beams. Int. J. Struct. Stab. Dyn. **14**, 1350056 (2014)
9. Pourasghar, A., Kamarian, S.: Dynamic stability analysis of functionally graded nanocomposite non-uniform column reinforced by carbon nanotube. J. Vib. Control **21**, 2499–2508 (2015)
10. Rafiee, M., Yang, J., Kitipornchai, S.: Thermal bifurcation buckling of piezoelectric carbon nanotube reinforced composite beams. Comput. Math. Appl. **66**, 1147–1160 (2013)
11. Yas, M.H., Samadi, N.: Free vibrations and buckling analysis of carbon nanotube-reinforced composite Timoshenko beams on elastic foundation. Int. J. Press. Vessels Pip. **98**, 119–128 (2012)
12. Ansari, R., Faghih Shojaei, M., Mohammadi, V., Gholami, R., Sadeghi, F.: Nonlinear forced vibration analysis of functionally graded carbon nanotube-reinforced composite Timoshenko beams. Compos. Struct. **113**, 316–327 (2014)
13. Ke, L.L., Yang, J., Kitipornchai, S.: Nonlinear free vibration of functionally graded carbon nanotube-reinforced composite beams. Compos. Struct. **92**, 676–683 (2010)
14. Shen, H.S., Xiang, Y.: Nonlinear analysis of nanotube-reinforced composite beams resting on elastic foundations in thermal environments. Eng. Struct. **56**, 698–708 (2013)
15. Rafiee, M., Yang, J., Kitipornchai, S.: Large amplitude vibration of carbon nanotube reinforced functionally graded composite beams with piezoelectric layers. Compos. Struct. **96**, 716–725 (2013)
16. Ke, L.L., Yang, J., Kitipornchai, S.: Dynamic stability of functionally graded carbon nanotube-reinforced composite beams. Mech. Adv. Mater. Struct. **20**, 28–37 (2013)
17. Alibeigloo, A., Liew, K.M.: Elasticity solution of free vibration and bending behavior of functionally graded carbon nanotube-reinforced composite beam with thin piezoelectric layers using differential quadrature method. Int. J. Appl. Mech. **7**, 1550002 (2015)
18. Yang, J., Ke, L.L., Feng, C.: Dynamic buckling of thermo-electro-mechanically loaded FG-CNTRC beams. Int. J. Struct. Stab. Dyn. **15**, 1540017 (2015)
19. Jam, J.E., Kiani, Y.: Low velocity impact response of functionally graded carbon nanotube reinforced composite beams in thermal environment. Compos. Struct. **132**, 35–43 (2015)
20. Mirzaei, M., Kiani, Y.: Snap-through phenomenon in a thermally postbuckled temperature dependent sandwich beam with FG-CNTRC face sheets. Compos. Struct. **134**, 1004–1013 (2015)
21. Wu, H., Kitipornchai, S., Yang, J.: Free vibration and buckling analysis of sandwich beams with functionally graded carbon nanotube-reinforced composite face sheets. Int. J. Struct. Stab. Dyn. **15**, 1540011 (2015)
22. Zhang, L.W., Song, Z.G., Liew, K.M.: State-space Levy method for vibration analysis of FG-CNT composite plates subjected to in-plane loads based on higher-order shear deformation theory. Compos. Struct. **134**, 989–1003 (2015)
23. Zhang, L.W., Cui, W.C., Liew, K.M.: Vibration analysis of functionally graded carbon nanotube reinforced composite thick plates with elastically restrained edges. Int. J. Mech. Sci. **103**, 9–21 (2015)
24. Lei, Z.X., Zhang, L.W., Liew, K.M.: Free vibration analysis of laminated FG-CNT reinforced composite rectangular plates using the kp-Ritz method. Compos. Struct. **127**, 245–259 (2015)
25. Lei, Z.X., Zhang, L.W., Liew, K.M.: Elastodynamic analysis of carbon nanotube-reinforced functionally graded plates. Int. J. Mech. Sci. **99**, 208–217 (2015)
26. Zhang, L.W., Liew, K.M.: Large deflection analysis of FG-CNT reinforced composite skew plates resting on Pasternak foundations using an element-free approach. Compos. Struct. **132**, 974–983 (2015)
27. Zhang, L.W., Song, Z.G., Liew, K.M.: Nonlinear bending analysis of FG-CNT reinforced composite thick plates resting on Pasternak foundations using the element-free IMLS-Ritz method. Compos. Struct. **128**, 165–175 (2015)
28. Zhang, L.W., Liew, K.M.: Geometrically nonlinear large deformation analysis of functionally graded carbon nanotube reinforced composite straight-sided quadrilateral plates. Comput. Methods Appl. Mech. Eng. **295**, 219–239 (2015)
29. Zhang, L.W., Lei, Z.X., Liew, K.M.: Buckling analysis of FG-CNT reinforced composite thick skew plates using an element-free approach. Compos. Part B Eng. **75**, 36–46 (2015)
30. Zhang, L.W., Liew, K.M., Reddy, J.N.: Postbuckling of carbon nanotube reinforced functionally graded plates with edges elastically restrained against translation and rotation under axial compression. Comput. Methods Appl. Mech. Eng. **298**, 1–28 (2016)
31. Lei, Z.X., Zhang, L.W., Liew, K.M., Yu, J.L.: Dynamic stability analysis of carbon nanotube-reinforced functionally graded cylindrical panels using the element-free kp-Ritz method. Compos. Struct. **113**, 328–338 (2014)
32. Lei, Z.X., Zhang, L.W., Liew, K.M.: Analysis of laminated CNT reinforced functionally graded plates using the element-free kp-Ritz method. Compos. Part B Eng. **84**, 211–221 (2016)
33. Shen, H.S.: Postbuckling of nanotube-reinforced composite cylindrical shells in thermal environments, part I: axially-loaded shells. Compos. Struct. **93**, 2096–2108 (2011)
34. Shen, H.S.: Thermal buckling and postbuckling behavior of functionally graded carbon nanotube-reinforced composite cylindrical shells. Compos. Part B Eng. **43**, 1030–1038 (2012)
35. Mirzaei, M., Kiani, Y.: Thermal buckling of temperature dependent FG-CNT reinforced composite conical shells. Aerosp. Sci. Technol. **47**, 42–53 (2015)
36. Mirzaei, M., Kiani, Y.: Thermal buckling of temperature dependent FG-CNT reinforced composite plates. Meccanica. doi:10.1007/s11012-015-0348-0
37. Mirzaei, M., Kiani, Y.: Free vibration of functionally graded carbon nanotube reinforced composite cylindrical panels. Compos. Struct. **142**, 45–56 (2016)
38. Jam, J.E., Kiani, Y.: Buckling of pressurized functionally graded carbon nanotube reinforced conical shells. Compos. Struct. **125**, 586–595 (2015)
39. Zhang, L.W., Lei, Z.X., Liew, K.M.: Buckling analysis of FG-CNT reinforced composite thick skew plates using an element-free approach. Compos. Part B Eng. **75**, 36–46 (2015)

40. Lei, Z.X., Zhang, L.W., Liew, K.M.: Vibration analysis of CNT-reinforced functionally graded rotating cylindrical panels using the element-free kp-Ritz method. Compos. Part B Eng. **77**, 291–303 (2015)
41. Zhang, L.W., Huang, D., Liew, K.M.: An element-free IMLS-Ritz method for numerical solution of three-dimensional wave equations. Comput. Methods Appl. Mech. Eng. **297**, 116–139 (2015)
42. Zhang, L.W., Zhu, P., Liew, K.M.: Thermal buckling of functionally graded plates using a local Kriging meshless method. Compos. Struct. **108**, 472–492 (2014)
43. Zhu, P., Zhang, L.W., Liew, K.M.: Geometrically nonlinear thermomechanical analysis of moderately thick functionally graded plates using a local Petrov Galerkin approach with moving Kriging interpolation. Compos. Struct. **107**, 298–314 (2014)
44. Zhang, L.W., Li, D.M., Liew, K.M.: An element-free computational framework for elastodynamic problems based on the IMLS-Ritz method. Eng. Anal. Bound. Elem. **54**, 39–46 (2015)
45. Ghiasian, S.E., Kiani, Y., Eslami, M.R.: Non-linear rapid heating of FGM beams. Int. J. Non Linear Mech. **67**, 74–84 (2014)
46. Prathap, G., Varadan, T.K.: The large amplitude vibration of hinged beams. Comput. Struct. **9**, 219–222 (1978)
47. Bhashyam, G.R., Prathap, G.: Galerkin finite element method for nonlinear beam vibrations. J. Sound Vib. **72**, 191–203 (1980)
48. Shen, H.S., Xiang, Y.: Postbuckling of axially compressed nanotube-reinforced composite cylindrical panels resting on elastic foundations in thermal environments. Compos. Part B Eng. **67**, 50–61 (2014)
49. Shen, H.S., Xiang, Y.: Postbuckling of nanotube-reinforced composite cylindrical shells under combined axial and radial mechanical loads in thermal environment. Compos. Part B Eng. **52**, 311–322 (2013)
50. Han, Y., Elliott, J.: Molecular dynamics simulations of the elastic properties of polymer/carbon nanotube composites. Comput. Mater. Sci. **39**, 315–323 (2007)
51. Wang, Z.X., Shen, H.S.: Nonlinear vibration and bending of sandwich plates with nanotube-reinforced composite face sheets. Compos. Part B Eng. **43**, 411–421 (2012)
52. Marur, S.R., Prathap, G.: Non-linear beam vibration problems and simplifications in finite element models. Comput. Mech. **35**, 352–360 (2005)